Multiple-electron capture processes in 70-keV $^{15}N^{7+}$ + Ar collisions: A triple-coincidence study

E. D. Emmons, A. A. Hasan, and R. Ali
Department of Physics, University of Nevada, Reno, Nevada 89557-0058
(Received 11 May 1999; revised manuscript received 19 July 1999)

Double- through quintuple-electron capture processes in the 70-keV $^{15}N^{7+}$ + Ar collision system have been investigated by means of time-of-flight triple-coincidence measurements of Auger electrons, scattered projectile, and target recoil ions. Subpartial Auger-electron spectra corresponding to specific pairs of final projectile and recoil-ion charge states have been obtained and discussed within the framework of the extended classical overbarrier model [A. Niehaus, J. Phys. B **19**, 2925 (1986)]. By allowing for target excitation, the model accounts reasonably well for the observed initial populations. Possible relaxation pathways of the populated multiply excited configurations have been identified. Measurements of this type allow a deeper understanding of the production and relaxation pathways of these configurations. [S1050-2947(99)06112-0]

PACS number(s): 34.70.+e, 34.50.Fa

I. INTRODUCTION

When a slow highly charged ion collides with a many-electron neutral gas target, many electrons can play a role in the resulting processes. The dominant process is the transfer of electrons from the target into excited states of the highly charged ion. The excited ion must then decay either radiatively or through the process of autoionization (if two or more electrons are captured) or through some combination of both processes. Single- and double-electron capture processes in such collisions are fairly well understood (see, e.g., [1–3] and references therein), but they still lend themselves to further investigations using a variety of techniques. In this respect, the new and powerful technique of cold-target recoil-ion momentum spectroscopy (COLTRIMS) [4–8] is acknowledged for providing new insights into these processes.

Although slow collisions involving more than two active electrons, and incident projectile charge states $q \geqslant 3$, have been investigated for over two decades, our understanding of multi-electron processes is far less than that of one- and two-electron processes. Experimentally, measurements of projectile charge-change [9–18], recoil-ion production [15–17,19], and total charge-transfer [15–17] cross sections, as well as cross sections differential in both recoil and final projectile charge states [15–17,20–27] have been reported. In addition, recoil charge state fractions have been measured in coincidence with final projectile charge states [28–31] and in a singles' mode [32,33]. A limited number of energy gain [31,34–40] and angular distribution and differential cross section [24,34,39,41–45] measurements involving more than double-electron capture have been carried out. Visible photon emission from Rydberg transitions in collisions of highly charged ions with many-electron targets [40,46–49] has also been investigated. Finally, Auger-electron spectroscopy has been employed in a singles' mode [50–52], in coincidence with target ions [53–57], and in time-of-flight (TOF) triple-coincidence with scattered projectile and target ions [58,59] to study such collisions.

Theoretically, quantum mechanical or semiclassical treatment of collisions involving more than two electrons is prohibitively difficult due to the large number of channels involved. In view of that, the simple classical overbarrier model [60] was extended [61,62] to account for multielectron processes. The extended classical overbarrier (ECB) model by Niehaus [62] distinguishes between two parts in the collision, the way in and the way out. On the way in, a number of target electrons become molecularized at different internuclear separations in order of increasing ionization potentials. On the way out, the molecularized electrons may be captured by the projectile or recaptured by the target. The model describes a single collision event by a string (j) whose elements are either 1 or 0 indicating capture by the projectile or recapture by the target, respectively, and where the positions of the elements label the electrons in order of increasing ionization potentials. For example, the string $(j) = (011)$ implies that three electrons are molecularized during the collision, out of which the electrons characterized by the second and third ionization potentials are captured by the projectile while the first is recaptured by the target. In this fashion, the model predicts electron capture to be accompanied by target excitation whenever initially loosely bound target electrons are recaptured by the target. The majority of the above-mentioned experimental measurements have been used to test the predictions of the ECB models [61,62] on cross sections for the removal of target electrons, energy gain, angular distribution of scattered projectiles, and Auger-electron spectra. Many of the predictions have been found in reasonable agreement with the experimental results. These models are limited to predicting the capture state distribution on the projectile and possible simultaneous target excitation. In order to further account for the final collision products, relaxation schemes for the multiply excited states must be invoked. There has been, until recently, a severe lack of theoretical work on the radiative and nonradiative properties of multiply excited states, due in part to the large number of states that need to be taken into account and in part to the lack of experimental data to which the calculations can be directly compared. Therefore, relaxation schemes [15,51,57] based on simple arguments, such as autoionization to the nearest continuum limits and minimum electron rearrangement (two-electron transitions), have been invoked. During the last few years, however, there has been increasing theoretical interest in the radiative and nonradiative properties of

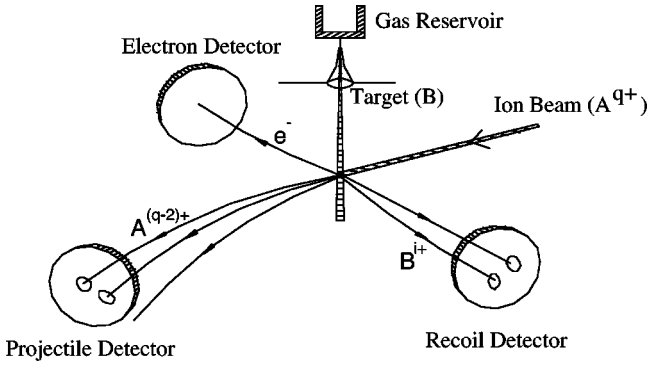

FIG. 1. A schematic of the experimental setup.

multiply excited states (see, e.g., [63–68], and references therein). In this respect, the recent investigations of triply excited lithium states using synchrotron radiation facilities (see, e.g., [69–71], and references therein) are acknowledged for stimulating additional theoretical interest in the properties of multiply excited states.

Since autoionization is the main decay mode of multiply excited states, Auger-electron spectroscopy should provide significant information on these states. While high resolution Auger-electron spectroscopy in a singles' mode has played a significant role in understanding two-electron processes (see, e.g., Ref. [72], and references therein), the situation is drastically different when many electrons are involved. The resulting spectra consist of superpositions of spectra derived from doubly, triply, quadruply, and possibly higher orders of multiply excited states. In the 70-keV $^{15}N^{7+}+Ar$ collision system in particular, Auger-electron spectroscopy has been used in both a singles' mode by Benoit-Cattin *et al.* [51] and in coincidence with recoil ions by de Nijs *et al.* [55]. Benoit-Cattin *et al.* [51] stated that even in the simplest case of this bare projectile ion, non-coincident spectra were difficult to interpret. On the other hand, de Nijs *et al.* [55] obtained partial Auger spectra corresponding to the different target ion charge states that are easier to interpret. Their measurements, however, were limited to electron energies less than 100 eV, and the discussion of three- and four-electron processes was rather brief. This article reports TOF triple-coincidence measurements of Auger electrons, scattered projectile, and target recoil ions in the 70-keV $^{15}N^{7+}+Ar$ collision system. The measurements provide subpartial Auger-electron spectra corresponding to specific final projectile and recoil-ion charge states that are easier to interpret. The spectra are discussed within the framework of the ECB model by Niehaus [62], and relaxation pathways of multiply excited configurations are discussed.

II. EXPERIMENT

A schematic of the experimental apparatus is shown in Fig. 1. The experiment was carried out at the University of Nevada, Reno, multicharged ion research facility. The $^{15}N^{7+}$ ions were produced by a 14-GHz electron cyclotron resonance (ECR) ion source [73] and extracted by a 10-kV potential. A mass-to-charge analyzing magnet was used to separate the nitrogen ions from other contaminants. The isotope ^{15}N was used to prevent contamination from bare helium and oxygen ions, which were also produced by the ion source. Next, the ions were guided to the interaction region where the ion beam crossed a supersonic Ar gas jet at 90°. The Ar jet was about 2 mm wide with an internal pressure of about 0.1 mTorr. Three detectors were used to detect the collision products. First, a small electric field ($\approx$10 V/cm) extracted the Ar recoil ions perpendicular to the incident ion beam. They were guided through a time-of-flight (TOF) spectrometer and were detected by a two-dimensional position-sensitive microchannel plate detector (2D-PSD). The position signals were not processed, however, since the spectrometer was optimized for TOF measurements only. Second, Auger electrons emitted at 90° relative to the incident ion beam traveled through another TOF spectrometer, located opposite to the recoil-ion spectrometer, and were detected by a microchannel plate detector. The spectrometer accepted electrons emitted at $90°\pm2.3°$ with respect to the incident ion beam direction. The electron spectrometer is magnetically shielded and contains a deceleration grid assembly that is used to obtain higher resolution electron spectra. A TOF spectrometer was used because it cuts down the need for scanning to only a few steps. In this particular experiment two steps were used. The first was with almost no electron deceleration so that *L*- and *M*-Auger electrons could be analyzed, and the second was with 315 volts of deceleration so that high-energy *K*-Auger electrons could be examined in higher resolution. Finally, the highly charged ion beam continued forward after the collision and then entered a region with a transverse electric field. The ions were deflected differently depending on their charge states. They struck another 2D-PSD and were detected. The collision chamber was differentially pumped in order to maintain high ion-beam purity both before entering the chamber and after leaving it. Pressures of about 4×10^{-9} and 1×10^{-8} Torr were maintained before and after the collision chamber, respectively, while the collision chamber pressure was about 1×10^{-7} Torr during the experiment. Double collisions were estimated to be less than 0.5%.

The experiment was done in TOF triple-coincidence mode. The data acquisition system was triggered by the detection of an electron or a photon. Since the electron detector views the interaction region, photons with energy higher than 12 eV that are emitted toward the detector will be detected. A fast timing signal derived from the electron detector was used to start a time-to-digital converter (TDC) which was stopped by a signal from the projectile detector. The electron TOF resolution was less than 2 ns and was dominated by the resolution of the detectors and associated electronics. The contributions of the projectile energy gain, and the difference in acceleration experienced by the different final projectile charge states as they left the recoil-ion extraction field region, to the TOF resolution were negligible compared to the electronic resolution. Another TDC was started by a fast signal from the projectile detector and stopped by a recoil signal. The position signals from the projectile detector were read by analog-to-digital (ADC) converters. The TOF of the recoil ions provided their charge states while the impact positions on the projectile 2D-PSD provided the final projectile charge states. The time and position information were stored in event mode for further processing. The true triple-coincidence rate was about 0.2 Hz for a primary ion-beam

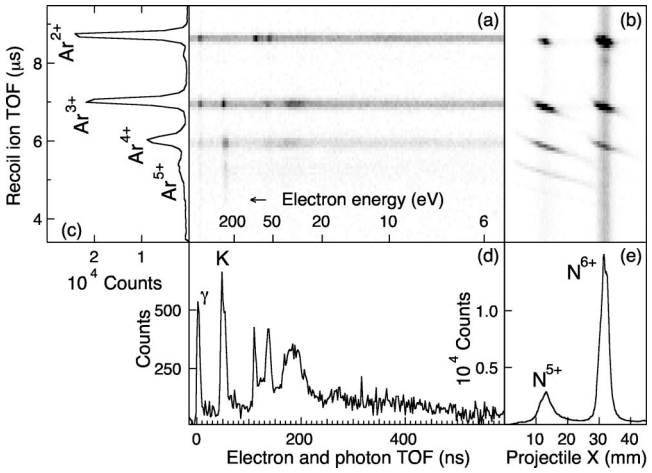

FIG. 2. A multiparameter representation of the triple-coincidence measurements. (a) Coincidences between recoil ions and Auger electrons or photons. (b) Coincidences between projectile and recoil ions. (c) Recoil-ion TOF spectrum. (d) Singles' Auger-electron/photon spectrum. The labels K and γ indicate K-Auger electrons and photons, respectively. (e) Final projectile charge-state distribution.

current of 2.5 pA. The data presented in this paper were collected in 60 h.

III. RESULTS AND DISCUSSION

Figure 2 is a multiparameter representation of the triple-coincidence measurements. Coincidences between recoil ions and Auger electrons or photons are represented by the scatter plot of Fig. 2(a), while coincidences between projectile and recoil ions are represented by that of Fig. 2(b). Projections onto the appropriate axes provide the recoil-ion TOF spectrum [Fig. 2(c)], the equivalent of a singles' Auger-electron spectrum [Fig. 2(d)], and the final projectile charge-state distribution [Fig. 2(e)]. It is evident that the singles' electron spectrum resulted from processes involving from two to five active electrons, and the interpretation of the spectrum would be a formidable task. However, partial Auger-electron spectra corresponding to the different recoil-ion charge states can be obtained by placing appropriate 2D windows in Fig. 2(a), and projecting the events within each window onto the horizontal axis. These partial spectra are shown in Fig. 3. Examination of Fig. 2(b), however, shows that these recoil ions are found in coincidence with projectile ions that changed their charge states by one or two units. This implies that the corresponding partial Auger spectra are still composite spectra, and therefore can be further reduced according to the final projectile charge states. This reduction will result in subpartial Auger spectra corresponding to specific pairs of final projectile and recoil-ion charge states. A figure similar to Fig. 2 can also be made for the higher resolution K-Auger-electron measurements (not shown here).

A. Double-electron capture

The partial Auger-electron spectrum in coincidence with Ar^{2+} recoil ions is shown in Fig. 3. The Auger line identification was carried out using the Hartree-Fock atomic structure code by Cowan [74]. A number of comments are in

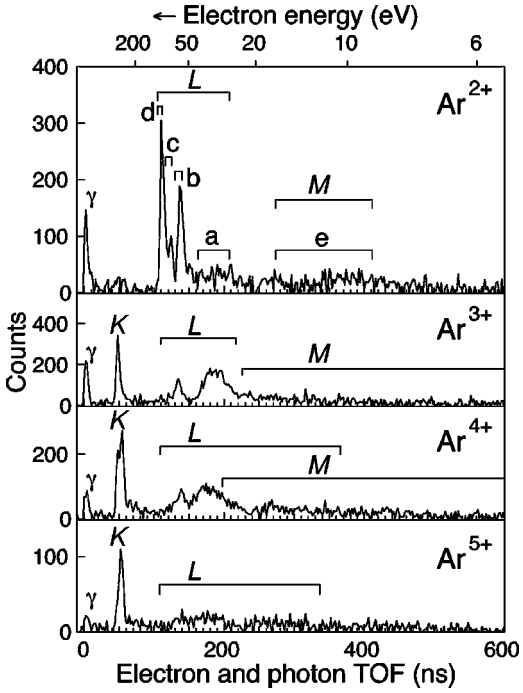

FIG. 3. Partial Auger-electron/photon spectra corresponding to the different recoil-ion charge states. The labels K, L, M, and γ indicate K-, L-, and M-Auger electrons and photons, respectively. The other labels in the Ar^{2+} spectrum correspond to the following Auger transitions: a: (3,3)→(2); b: (3,4)→(2); c: (3,5)→(2); d: (4,4)→(2); e: (4,5)→(3).

order. First, the L- and M-Auger-electron lines are consistent with the coincidence measurements of de Nijs *et al.* [55]. The main configurations that are populated in double-electron capture are (3,3), (3,4), (3,5), (4,4), and (4,5), with some $(3,n), n \geqslant 6$. Both measurements reveal significant populations of the (3,3) and (3,4) configurations, in contradiction with the conclusions of Benoit-Cattin *et al.* [51] that these states can be disregarded based on comparisons with Auger-electron spectra obtained in 70-keV $N^{7+}+He$, H_2 collisions. The reaction windows predicted by the ECB model [62] for double-electron capture are shown in Fig. 4 for a number of possible strings. It is clear that all the experimentally observed projectile doubly excited configurations can be accounted for by the model. The reaction window corresponding to the two-electron string $(j)=(011)$ overlaps the (4,4), (4,5), and $(3,n), n \geqslant 6$, configurations, and that corresponding to the three-electron string $(j)=(011)$ overlaps the (3,4) and (3,5) configurations, while the (3,3) configuration can only be accounted for by a four-electron string such as $(j)=(0011)$. According to the ECB model [62], the population of the (3,3), (3,4), and (3,5) configurations must then be accompanied by target excitation. de Nijs *et al.* [55] argued in favor of this interpretation based on similar comparisons with the model. Recently, Hasan *et al.* [75] have obtained direct experimental evidence, by means of simultaneous Auger-electron and COLTRIMS spectroscopic techniques, for significant target outer-shell excitation accompanying the population of these configurations in the 28-keV $^{15}N^{7+}+Ar$ collision system. Their findings are in support of the predictions of the ECB model [62] regarding target excitation. Since electron-capture processes in slow

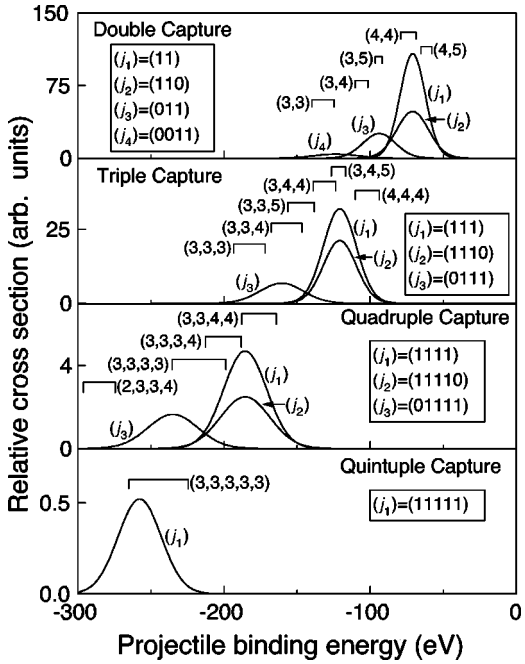

FIG. 4. Reaction windows predicted by the ECB model [62] for representative strings (j) (see the text for explanation) giving rise to double- through quintuple-electron capture. Other windows that lie in between the shown reaction windows are not shown. Also included are the total projectile binding energies obtained using the Cowan code [74] for various multiply excited configurations in nitrogen ions.

multiply charged ion-atom collisions are only weakly velocity dependent, we believe that the population of these configurations at the present collision energy of 0 keV is also accompanied by significant target excitation. This is in agreement with the conclusion of de Nijs *et al.* [55], but again in disagreement with the conclusion of Benoit-Cattin *et al.* [51] who argued that target excitation is not important. Double-electron capture processes therefore cannot be properly accounted for, within the framework of the ECB model [62], by two-electron processes. At least four-electron processes, where the target recoil-ion may be left in excited states depending on which electrons are captured by the projectile, are needed to properly account for all the observed doubly excited configurations. Assuming four electrons are molecularized during the collisions, the ECB model [62] predicts that nearly half the double-electron capture processes are accompanied by target excitation. The Auger-electron intensity under the labels ''a, b, and c'' in the Ar^{2+} partial spectrum accounts for nearly half the total intensity, in reasonable agreement with the prediction.

Second, we were able to determine that there are little or no K-Auger electrons coming from double-electron capture. de Nijs *et al.* [55] could not determine this because they did not look for electrons in this high-energy range. Benoit-Cattin *et al.* [51] could find electrons in this energy range, but because of the noncoincident nature of their experiment they could not tell if they came from double-electron capture or from autoionizing cascades from capture of three or more electrons. This absence of high-energy electrons is consistent with the general rule that autoionization preferentially occurs to the nearest continuum limits. Third, we note that the partial spectrum in coincidence with Ar^{2+} recoil ions closely resembles that obtained by Merabet *et al.* [58] in the 60-keV O^{7+} + Ar collision system. This indicates that, at least in the case of double-electron capture, electron capture processes in both systems are dominated by the incoming projectile charge state, and that the projectile core effect is negligible in the case of O^{7+}.

Finally, true double-electron capture (TDC) was seen only in coincidence with photons (spectrum not shown here), as expected, since it results from the radiative stabilization of both captured electrons. TDC in $^{15}N^{7+}$ + Ar collisions was studied by Roncin *et al.* [76,77] at 10.5-keV collision energy using a coincident energy gain technique. The TDC energy gain profile was found to consist of a narrow peak while that corresponding to autoionizing double-electron capture (ADC) was much broader. The TDC peak matched well with the population of the (4,4) doubly excited configuration. The ADC peak was also assumed to be dominantly associated with the (4,4) configuration, and they attributed the much broader profile to the kinematic broadening caused by autoionization. The radiative stabilization probability (P_{rad}), which is the ratio of the TDC intensity to the total double-electron capture intensity, was about 40%. This value is much higher than expected, however, since the states belonging to the (4,4) configuration are expected to dominantly autoionize. To explain the high P_{rad}, the initially populated (4,4) configuration was assumed to undergo a population transfer to the quasidegenerate, and highly asymmetric, Rydberg series $(3,n>9)$. This population transfer is thought to be induced by a postcollision interaction mechanism known as the autotransfer to Rydberg states (ATR) [77,78]. The highly asymmetric Rydberg states were believed to have a large fluorescence yield, thus explaining the high P_{rad}. The direct observation of photon emission from Rydberg transitions following multiple-electron capture collisions [46–48] further supported the argument that populating highly asymmetric Rydberg states plays an important role in realizing radiative stabilization of both electrons. Roncin *et al.* [77] developed an analytical model for the subsequent decay of the Rydberg states. They found that the ATR mechanism can actually be very efficient, but autoionization of the Rydberg states is more important than originally assumed. Nevertheless, they found that radiative stabilization was due to the large fluorescence yield of the high-lying Rydberg States. For the 10.5-keV $^{15}N^{7+}$ + Ar collision system, the model P_{rad} was about 20%, a factor of two below the experimental result. Another improvement came about by incorporating the postcollisional increase of the angular momentum of the Rydberg electron into the ATR model [79]. It was found that this increase is fast enough to quench the autoionization process, thus increasing P_{rad}, and that P_{rad} is strongly velocity dependent. Large average P_{rad} values, even larger than the experimental value, have been obtained.

In the present measurements, we cannot distinguish the Rydberg electrons resulting from autoionization of the $(3,n>9)$ configurations from those resulting from the (4,4) configuration due to their substantial energy overlap and to the limited resolution. From a separate measurement of the recoil-ion charge state fractions in coincidence with the final projectile charge states at 70 keV, however, we have determined a value of 20% for P_{rad}. This value, being smaller

than that reported by Roncin *et al.* [76,77] at 10.5 keV, is in general agreement with the velocity dependence of P_{rad} [79]. As mentioned earlier, however, Hasan *et al.* [75] have obtained direct experimental evidence that the (3,3), (3,4), and (3,5) configurations are also populated in the 28-keV $^{15}N^{7+}$ + Ar collision system, and that their population is accompanied by significant target excitation. The net energy gain associated with the population of these configurations significantly overlaps that associated with the pure population of the (4,4) configuration and contributes to the broadening of the ADC energy gain profile. Although Hasan *et al.* [75] performed their measurements at 28 keV ($v \approx 0.27$ a.u.) while Roncin *et al.* [76,77] at 10.5 keV ($v \approx 0.17$ a.u.), the relative population of the different configurations is not expected to change significantly. In fact, the partial Auger-electron spectrum in coincidence with Ar^{2+} recoil ions obtained by Hasan *et al.* [75] is nearly identical with the one obtained in our present measurements at 70 keV ($v \approx 0.43$ a.u.), and shows little velocity dependence. In our opinion, it is impossible to accurately obtain the relative population of the different configurations in the coincident energy gain measurements [76,77]. We therefore believe that P_{rad} for the initially populated (4,4) configuration, after undergoing ATR population transfer, is probably twice as large as the value reported by Roncin *et al.* [76,77] for the 10.5-keV collision energy. A similar conclusion has been reached by de Nijs *et al.* [55]. This conclusion favors the model which takes into account the increase of the angular momentum of the Rydberg electron [79].

B. Triple-electron capture

The partial Auger-electron spectrum in coincidence with Ar^{3+} recoil ions is also shown in Fig. 3. This spectrum is clearly different from that corresponding to Ar^{2+} recoil ions, with one distinct difference being the presence of *K*-Auger electrons. We will not attempt, however, to analyze this spectrum since an examination of Fig. 2(b) shows that Ar^{3+} recoil ions are found in coincidence with projectile ions that changed their charge states by one or two units. This implies that the Ar^{3+} partial spectrum can be further reduced to subpartial spectra associated with the different final projectile charge states. Subpartial Auger spectra in coincidence with the (Ar^{3+}, N^{6+}) and (Ar^{3+}, N^{5+}) ion pairs are shown in Fig. 5. The reaction windows predicted by the ECB model [62] for triple-electron capture are shown in Fig. 4 for a number of possible strings. Assuming only three electrons are molecularized in the collision, triple-electron capture is described by the string $(j)=(111)$ and the model predicts a primary population of the (4,4,4) and $(3,4,n_3=4,5)$ configurations. It is well known that with increasing number of captured electrons the population shifts toward lower-lying levels on the projectile, and judging from the observed double-electron capture population we believe that the (4,4,4) is an unlikely configuration and will therefore be disregarded. Furthermore, all states belonging to the $(3,4,n_3=4,5)$, configurations are energetically allowed to autoionize to the (3,3) continuum limits and will preferentially do that. We are ignoring, here, possible population transfer to the $(3,3,n \gg 4)$ Rydberg series via the ATR mechanism which will be discussed later. The (3,3) configuration in turn will autoionize

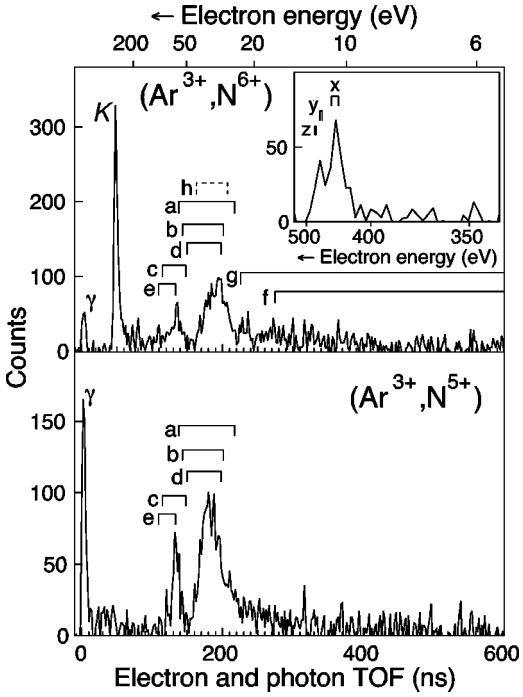

FIG. 5. Subpartial Auger-electron/photon spectra in coincidence with the (Ar^{3+}, N^{6+}) (top) and (Ar^{3+}, N^{5+}) (bottom) ion pairs. Inset: A moderate resolution *K*-Auger-electron spectrum in coincidence with the (Ar^{3+}, N^{6+}) ion pair. The labels correspond to the following Auger transitions: *a*: (3,3,3)→(2,3); *b*: (3,3,4)→(2,4); *c*: (3,3,4)→(2,3); *d*: (3,3,5)→(2,5); *e*: (3,3,5)→(2,3); *f*: (3,4,4)→(3,3); *g*: (3,4,5)→(3,3); *h*: (3,3)→(2); *x*: (2,3)→(1); *y*: (2,4)→(1); *z*: (2,5)→(1). The electron TOF ranges, in the main spectra, are shown in solid lines for the first autoionization steps and in dashed lines for the second autoionization steps.

to the $n=2$ continuum limits, thus resulting in the retention of only one electron by the projectile. We should therefore expect to see electrons associated with the $(3,4,n_3=4,5) \rightarrow (3,3)$ transitions in the subpartial spectrum corresponding to the (Ar^{3+}, N^{6+}) ion pair. Indeed, such electrons are observed in that spectrum and are labeled by *f* and *g*. Their intensity, however, is considerably smaller than what would be expected from the ECB model [62]. While the autoionizing $(3,4,n_3=4,5) \rightarrow (2,n=3-5)$ transitions are also possible, the resulting Auger-electron energies are substantially larger than those associated with transitions to the (3,3) continuum limits. The intensity of these electrons should therefore be much smaller than those labeled *f* and *g*, since autoionization prefers the least change in energy, and will therefore be disregarded throughout the rest of the discussion.

Aside from the *K*-Auger-electron peak in the (Ar^{3+}, N^{6+}) subpartial spectrum, both subpartial spectra are dominated by electrons associated with the initial population of the $(3,3,n_3=3-5)$ triply excited configurations. As shown in Fig. 4, the ECB model [62] predicts significant population of these configurations only via at least four-electron processes, such as that represented by the string $(j)=(0111)$, where the target is left in excited states. Clearly, the model can successfully account for the observed populated configurations; however, the relative intensities are not properly accounted for. The model predicts nearly equal population for

the $(3,4,n_3=4,5)$ and the $(3,3,n_3=3-5)$ configurations, the latter are accompanied by target excitation while the former are not. This is clearly not the case as can be seen in Fig. 5.

Auger electrons resulting from the autoionizing $(3,3,n_3=3-5)\rightarrow(2,n=3-5)$ transitions are common to both subpartial spectra. Whether an event results in the (Ar^{3+}, N^{6+}) ion pair or the (Ar^{3+}, N^{5+}) ion pair is then determined by the competition between the radiative and autoionization decay modes of the resulting doubly excited states (see, e.g., Ref. [80], and references therein). The (Ar^{3+}, N^{5+}) spectrum is therefore a pure spectrum involving one autoionization step only, while the (Ar^{3+}, N^{6+}) spectrum is still a composite one resulting from the autoionization of the triply and subsequent doubly excited configurations. While autoionization of the $(2,n=3-5)$ doubly excited configurations involves the emission of *K*-Auger electrons that are well separated in energy from the autoionization electrons of the triply excited configurations, the (3,3) configuration autoionizes with the emission of electrons that overlap those from the $(3,3,n_3=3-5)$ configurations, thus further complicating the analysis of the (Ar^{3+}, N^{6+}) spectrum. *K*-Auger electrons are essentially absent in the (Ar^{3+}, N^{5+}) spectrum, indicating that *K*-Auger electrons are not emitted in the first autoionization step which is consistent with the assumption of the dominance of autoionization to the nearest continuum limits. In the first autoionization step, the (3,3,3) configuration autoionizes to the (2,3) continuum limits, while the $(3,3,n_3=4,5)$ can autoionize to the (2,3) or the $(2,n=4,5)$ continuum limits. It is clear that autoionization of the $(3,3,n_3=4,5)$ configurations to the associated $(2,n=4,5)$ continuum limits is more probable than to the (2,3) limits. In autoionizing to both continuum limits, the $(3,3,n_3=4,5)$ configurations give rise to electrons that overlap in energy. Furthermore, the $(3,3,n_3=4,5)\rightarrow(2,n=4,5)$ transitions give rise to electrons that overlap those from the $(3,3,3)\rightarrow(2,3)$ transitions, thus rendering the relative initial populations impossible to obtain from the (Ar^{3+}, N^{5+}) spectrum. Examination of the inset of Fig. 5, which is a moderate resolution *K*-Auger-electron spectrum obtained in coincidence with the combination (Ar^{3+}, N^{6+}), reveals that both the (2,4) and (2,5) configurations have been populated following the first autoionization step. However, due to the limited resolution and statistical precision, we refrain from attempting to obtain the relative initial populations from this spectrum. Instead, we will discuss the radiative and nonradiative properties of the combined $(3,3,n_3=4,5)$, configurations.

We consider first the branching ratios for radiative and autoionizing decays of the doubly excited daughter states. Taking the ratio of the Auger line intensities under the labels *c* and *e* in the (Ar^{3+}, N^{6+}) spectrum to the total intensity under the same labels in both spectra, one obtains an average *K*-Auger yield $a_K\approx0.5$ for the (2,3) doubly excited configuration. Stolterfoht *et al.* [81] calculated an average Auger yield $a_K=0.66$ for the singlet states belonging to the $2l3l'$ configuration in C^{4+}. Applying the scaling laws for radiative and autoionization rates [82] we obtain the average yield $a_K=0.55$ for the same $2l3l'$ configuration in N^{5+}. This value is in good agreement with our experimental value considering that in the present case the doubly excited states resulted from the autoionization of triply excited states and not directly populated in the collisions, and that there are no restrictions that prevent triplet states from being populated. A similar yield cannot be accurately obtained for the combined (2,4) and (2,5) configurations due to the overlap between the *a*, *b*, *d*, and *h* electrons in the (Ar^{3+}, N^{6+}) spectrum, and between the *a*, *b*, and *d* electrons in the (Ar^{3+}, N^{5+}) spectrum. We can be certain, however, that it is less than 0.5.

For similar reasons, accurate branching ratios for autoionization of the $(3,3,n_3=4,5)$ configurations to the different continuum limits are difficult to obtain. We can, however, try to estimate approximate ratios. The right-hand shoulder of the electron distribution under the labels *a*, *b*, and *d* in the (Ar^{3+}, N^{5+}) spectrum seems to result from the (3,3,3) $\rightarrow$(2,3) transitions. If we assume that the actual contribution of the $(3,3,3)\rightarrow(2,3)$ transitions is roughly twice the area under the shoulder, and then subtract that contribution from each subpartial spectrum, we obtain the contributions of the other transitions. Equal $(3,3,3)\rightarrow(2,3)$ contributions can be assumed for both spectra because $a_K\approx0.5$ for the (2,3) doubly excited daughter configuration. By then taking the ratio of the remaining intensity under the labels *b*, *d*, and *h* in both subpartial spectra to the remaining intensity under *b*, *c*, *d*, *e*, and *h* in both spectra, we obtain an autoionization branching ratio of $\approx$ 0.72 for the $(3,3,n_3=4,5)\rightarrow(2,n=4,5)$ transitions. This is to be considered as an approximate upper limit since the electrons associated with the transition *h* should not be counted. This value implies an approximate lower limit on the branching ratio for the $(3,3,n_3=4,5)\rightarrow(2,3)$ transitions of ≈0.28. It is to be stressed here that these approximate branching ratios are for the combined $(3,3,n_3=4,5)$ configurations. Vaeck and Hansen [63] investigated the properties of some of the triply excited configurations in N^{4+} using the single configuration average (SCA) method. For the $3s3p4d$ triply excited states, one can extract autoionization branching ratios of ≈0.29 to the (2,3) continuum limits and ≈0.71 to the (2,4) continuum limits. The apparent excellent agreement is probably fortuitous considering the crudeness of our estimates, and that the data reflect the possible population of a large number of states belonging to the $(3,3,n_3=4,5)$ configurations. We would rather say that our estimates are in line with their calculations. It is worth mentioning here that while the absence of *K*-Auger electrons in the (Ar^{3+}, N^{5+}) spectrum is consistent with the widely used assumption of the dominance of autoionization to the nearest continuum limits, the data show clear deviations from this assumption when several other continuum limits are available. Figure 6 summarizes our main findings for triple-electron capture in the form of relaxation pathways. The starting points are what we believe to be the dominant initial triply excited configurations. Branching ratios and Auger yields are noted on the figure whenever possible.

The previous discussion did not take into account possible postcollision interactions leading to the population of triply excited Rydberg states. In an extension of the ATR mechanism to triple-electron capture, Roncin *et al.* [39] argued that the initially populated (3,4,4) configuration, in the 10.5-keV $^{15}N^{7+}$ + Ar collision system, undergoes population transfer to the $(3,3,n\gg4)$ Rydberg series. The Rydberg states will then primarily autoionize to the $(2,n\gg4)$ continuum limits. The $(2,n\gg4)$ configurations are then assumed to dominantly radiatively stabilize. This scenario has been invoked [39] to

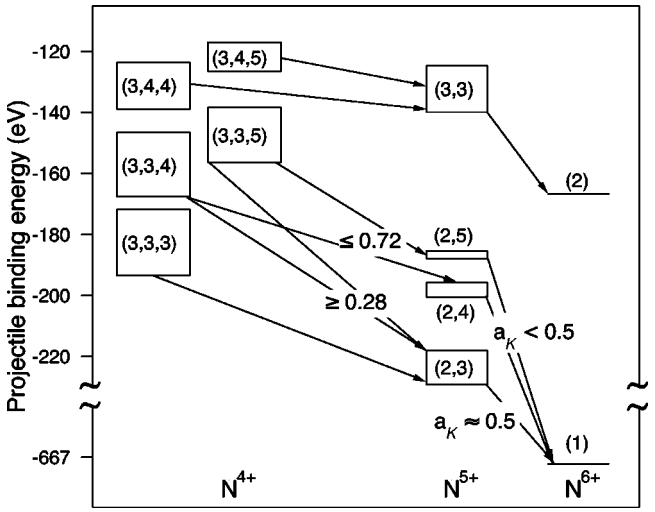

FIG. 6. Dominant initial populations and subsequent relaxation pathway following triple-electron capture.

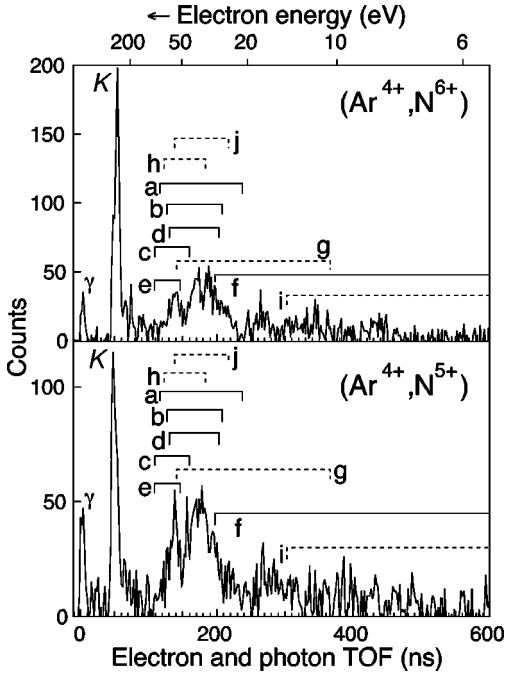

FIG. 7. Subpartial Auger-electron/photon spectra in coincidence with the (Ar^{4+}, N^{6+}) (top) and (Ar^{4+}, N^{5+}) (bottom) ion pairs. The labels correspond to the following Auger transitions: *a*: (3,3,3,3)→(2,3,3); *b*: (3,3,3,4)→(2,3,4); *c*: (3,3,3,4)→(2,3,3); *d*: (3,3,4,4)→(2,4,4); *e*: (3,3,4,4)→(2,3,4); *f*: (3,3,4,4)→(3,3,3); *g*: (2,3,3)→(2,2); *h*: (2,3,4)→(2,2); *i*: (2,4,4)→(2,3); *j*: (3,3,3)→(2,3). The electron TOF ranges are shown in solid lines for the first autoionization steps and in dashed lines for the second autoionization steps.

explain the high ratio of the (Ar^{3+}, N^{5+}) to the (Ar^{3+}, N^{6+}) ion pair yields, which was about 1.8. In their analysis they assumed a dominant initial population of the (3,4,4) configuration. At the present collision energy of 70 keV, and from a separate measurement of the recoil-ion charge state fractions in coincidence with the final projectile charge states, we have determined this ratio to be 1.25. It was shown earlier that the subpartial Auger-electron spectra in coincidence with both ion pairs in Fig. 5 are dominated by electrons associated with the initial population of the $(3,3,n_3=3-5)$ triply excited configurations. It was also shown that, following the first autoionization step, retaining one or two electrons is, for the most part, determined by the competition between the radiative and autoionization decay modes of doubly excited daughter configurations of the form $(2,n=3-5)$. It should be stressed here that the $(2,n=3-5)$ configurations have large average fluorescence yields ($\geqslant 0.45$). Furthermore, like double-electron capture, a significant fraction of triple-electron capture is expected to be accompanied by target excitation. The highly probable target excitation, and the severe limitation on resolution due to kinematic broadening, make it impossible to accurately obtain the relative population of the different initial configurations in the coincident energy gain measurements [39]. In addition, the measurements of Hasan *et al.* [75] indicate that, even in the case of triple-electron capture, the subpartial Auger-electron spectra show little velocity dependence. We therefore do not expect a significant change in the relative population of the different configurations at 10.5 keV. The conclusion of Roncin *et al.* [39], that retention of two electrons is mainly due to the initial population of the (3,4,4) configuration followed by population transfer to the $(3,3,n\gg 4)$ Rydberg series, is therefore called into question. In fact, if this were the main pathway for the retention of two electrons, the (Ar^{3+}, N^{5+}) subpartial spectrum in Fig. 5 should contain only one peak corresponding to the $(3,3,n\gg 4)\rightarrow(2,n\gg 4)$ transitions. Clearly, this is not the case. While we do not exclude the ATR scenario as a possible pathway for the retention of two electrons, we do not believe that it is as important as reported by Roncin *et al.* [39]. We would like to stress that the difference in interpretation derives from the difference in the identification of the initially populated configurations and their relative intensities.

C. Quadruple-electron capture

Figure 2(b) shows that Ar^{4+} recoil ions are also found in coincidence with both N^{6+} and N^{5+} ions, and therefore the corresponding partial spectrum in Fig. 3 can be further reduced to subpartial spectra. These subpartial spectra are shown in Fig. 7. We note that *K*-Auger electrons are now observed in both spectra, and that the low-energy electron distributions are nearly similar in both spectra. The *K*-Auger-electron distributions are quite different, however, as can be seen in Fig. 8. These *K*-Auger electrons are clearly the result of autoionizing cascades and not from quadruply excited states. The ECB model [62] predicts that the primary configurations initially populated in quadruple-electron capture are the (3,3,3,3), (3,3,3,4), and (3,3,4,4) configurations, as implied by the reaction windows shown in Fig. 4 for some of the possible strings. The two subpartial spectra show two distinct low-energy electron groups in the range 100–200 ns. The more energetic group matches well with the (3,3,3,4)→(2,3,3) and (3,3,4,4)→(2,3,4) transitions, labeled *c* and *e*, respectively. The less energetic group matches with the (3,3,3,4)→(2,3,4) and (3,3,4,4)→(2,4,4) transitions, labeled *b* and *d*, respectively. In addition, the (3,3,3,3)→(2,3,3) transitions, labeled *a*, produce electrons that could contribute to both of these groups. The (3,3,4,4)→(3,3,3) transitions are also possible giving rise to the electrons la-

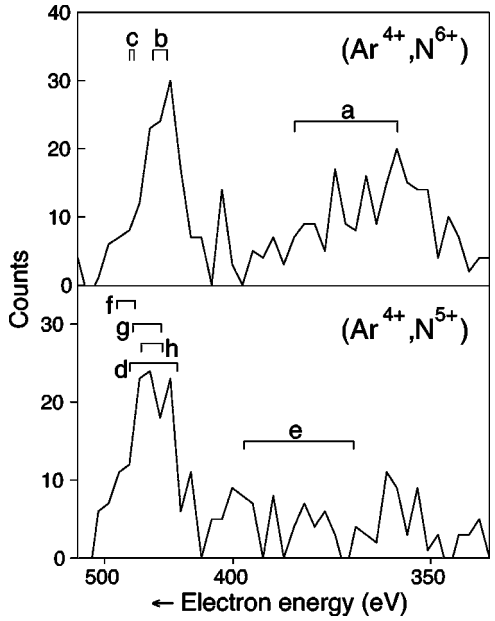

FIG. 8. Moderate resolution *K*-Auger-electron spectra in coincidence with the (Ar^{4+}, N^{6+}) (top) and (Ar^{4+}, N^{5+}) (bottom) ion pairs. The labels correspond to the following Auger transitions: *a*: (2,2)→(1); *b*: (2,3)→(1); *c*: (2,4)→(1); *d*: (2,2,3)→(1,2); *e*: (2,2,3)→(1,3); *f*: (2,3,4)→(1,3); *g*: (2,3,3)→(1,3); *h*: (2,3,4)→(1,4).

beled *f*. Coster-Kronig-type transitions such as (3,3,3,4)→(3,3,3) are also possible for some of the initially populated quadruply excited states. Most of these Coster-Kronig electrons have very low energies (<5 eV) and cannot be detected in our experiment. It should be mentioned, however, that only a small fraction of the states belonging to the quadruply excited configurations can undergo Coster-Kronig transitions, and therefore such transitions will be disregarded. The subpartial spectra are further complicated by electrons from the autoionization of the triply excited daughter configurations. The transitions labeled *g*, *h*, *i*, and *j* are the most important transitions originating in the triply excited configurations that are consistent with the initially populated quadruply excited configurations. While the transitions *g* and *i*, together with *f*, account for the low-energy electron distributions, beyond 230 ns, the transitions *h* and *j* clearly produce electrons that overlap in energy with those from the initially quadruply excited configurations.

Assuming that our identification of the dominant initial population of the (3,3,3,3), (3,3,3,4), and (3,3,4,4) configurations is indeed correct, we should not expect any contribution to the low-energy electron distributions from ''third generation'' doubly excited configurations. These configurations will either autoionize emitting a high-energy *K*-Auger electron or radiatively stabilize in which case no electrons will be emitted. This does not mean, however, that *K*-Auger electrons come only from doubly excited configurations, but may also be produced in the autoionization of triply excited configurations. In fact, the two *K*-Auger electron spectra in Fig. 8 provide further insights into the relaxation pathways. The *K*-Auger electrons corresponding to the (Ar^{4+}, N^{6+}) ion pair in Fig. 8 result from only the last step in the autoionization cascade starting from the initially populated quadruply excited configurations. If a triply excited configuration emitted a *K*-Auger-electron the event would not belong to this spectrum. The spectrum is dominated by the (2,2)→(1) and (2,3)→(1) transitions. There seems to be much weaker (2,4)→(1) transitions as well. We should search for pathways for the production of these $(2,n)$ configurations. It has already been seen that the triply excited configurations (2,3,3), (2,3,4), (2,4,4), and (3,3,3) are produced in the first autoionization steps. All but (3,3,3) can autoionize to the (2,2) continuum limits. The (2,2) configuration can therefore be accessed from all the initially populated quadruply excited configurations. Interestingly, Benoit-Cattin *et al.* [51] speculated that the (2,2) line should be observed in quadruple-electron capture and not in triple-electron capture. We can now definitively confirm this, since the (2,2) line was not seen in coincidence with triple-electron capture. On the other hand, the (2,3) doubly excited configuration can only be produced from the initial (3,3,4,4) configuration via the (3,3,4,4)→(2,4,4)→(2,3) and (3,3,4,4)→(3,3,3)→(2,3) autoionizing cascades. We are ignoring a possible small contribution from the (3,3,3,4)→(3,3,3)→(2,3) cascade which is initiated by a first step Coster-Kronig transition. The observed (2,3) population therefore constitutes evidence for the initial population of, at least, the (3,3,4,4) configuration since configurations of lesser excitation cannot significantly feed the (2,3) configuration. This conclusion is further supported by the observed electrons under label *e* in the subpartial spectra of Fig. 7.

The *K*-Auger spectrum in coincidence with the (Ar^{4+}, N^{5+}) ion pair in Fig. 8 has one distinct group of electrons. These electrons could be identified with the (2,3,3)→(1,3), (2,3,4)→(1,3), and (2,3,4)→(1,4) transitions, or with the (2,2,3)→(1,2) transitions. The former transitions are consistent with the initial population of the quadruply excited configurations discussed earlier, while the latter require initial populations of the form $(2,n_2,n_3,n_4)$ with $n_2,n_3,n_4 \geqslant 3$. Judging from the close similarity of the low-energy electron distributions in the two subpartial spectra of Fig. 7, however, we believe that the initial quadruply excited configurations giving rise to both spectra are the same for the most part. Furthermore, if indeed the (2,2,3) triply excited configuration is dominantly responsible for the observed *K*-Auger electrons, we should expect to see even more electrons resulting from the (2,2,3)→(1,3) transitions as will be clearly shown when discussing quintuple-electron capture. There are a few electrons that can be ascribed to the (2,2,3)→(1,3) transitions; however, their intensity is less than what would be expected. While we cannot exclude the initial population of the $(2,n_2,n_3,n_4)$ configurations, we believe that it is weak, and that a significant fraction of the observed *K*-Auger electrons is derived from the initial configurations discussed earlier via autoionizing cascades. The previous argument also finds support in the ECB model [62] predictions. Reasonable values for n_2, n_3, and n_4 that are in line with the observed initial populations for double-, triple-, and the majority of quadruple-electron capture result in configurations that can be only weakly populated according to the model. For example, the (2,3,3,4) configuration is nearly completely outside the reaction window corresponding to the string $(j)=(01111)$, which is a five-electron string, as can be seen in Fig. 4. This makes direct population of $n=2$ in quadruple-electron capture rather a weak process.

The previous discussion leads us to tentatively assign a significant fraction of the observed *K*-Auger electrons to the $(2,3,3)\rightarrow(1,3)$, $(2,3,4)\rightarrow(1,3)$, and $(2,3,4)\rightarrow(1,4)$ transitions. If that is indeed the case, these transitions would represent significant deviations from the criterion of autoionization to the nearest continuum limits. Theoretical investigations of the radiative and nonradiative properties of the (2,3,3) and (2,3,4) triply excited configurations would definitely help elucidate this issue. Answers may also be found by simultaneously measuring the *Q* value of these collisions.

As a final remark we note that, at variance with the case of triple-electron capture, retention of two electrons by the projectile following quadruple-electron capture is realized following two main pathways. The first involves the radiative stabilization of ''third generation'' doubly excited configurations of the form $(2,n=2-4)$. The second pathway involves the filling of a *K*-shell vacancy in the autoionization process of triply excited daughter configurations of the form $(2,3,n=3,4)$. Of course, the second pathway involves the emission of a *K*-Auger electron, and the N^{5+} projectile ion is left in a singly excited state. Although the ATR mechanism may lead to the population of Rydberg states, and indeed visible photons from Rydberg electron transitions have been observed in multiple-electron capture collisions [40,46–49], the role played by such states in the retention of two electrons in this case does not seem to be significant. This conclusion is justified by the very close similarity of the two subpartial spectra in coincidence with the (Ar^{4+}, N^{6+}) and (Ar^{4+}, N^{5+}) ion pairs, and by the success in accounting for their main features starting with the aforementioned initial populations.

D. Quintuple-electron capture

Electrons were also observed in coincidence with Ar^{5+} recoil ions as can be seen in Fig. 2. The intensity was much lower than for other recoil-ion charge states, however. They were found in coincidence with only N^{5+} projectile ions. Benoit-Cattin *et al.* [51] stated that they found nothing in the singles' electron spectrum concerning quintuple-electron capture, and de Nijs *et al.* [55] did not discuss these processes either. For convenience, the partial Auger spectrum in coincidence with Ar^{5+} recoil ions is shown again in Fig. 9 together with a higher resolution *K*-Auger spectrum. The ECB model [62] predicts a reaction window for the string $(j)=(11111)$ that overlaps the (3,3,3,3,3) quintuply excited configuration as can be seen in Fig. 4. Low-energy electrons are then expected from the $(3,3,3,3,3)\rightarrow(2,3,3,3)\rightarrow(2,2,3)$ autoionizing cascades. Indeed, these transitions match well with the majority of the low-energy electrons as can be seen in Fig. 9. *K*-Auger electrons are then expected from the $(2,2,3)\rightarrow(1,3)$ and $(2,2,3)\rightarrow(1,2)$ transitions. Such electrons are indeed the dominant ones as can be seen in the inset of Fig. 9. The relative intensities of the *K*-Auger electrons are consistent with what one would expect. There are slightly more electrons resulting from the $(2,2,3)\rightarrow(1,3)$ than from the $(2,2,3)\rightarrow(1,2)$ transitions. This was not the case in quadruple-electron capture, which further supports our previous discussion of quadruple-electron capture. We did not consider other strings or other quintuply excited configurations since the major features of the low-energy and *K*-Auger spectra are accounted for starting with the (3,3,3,3,3) configuration.

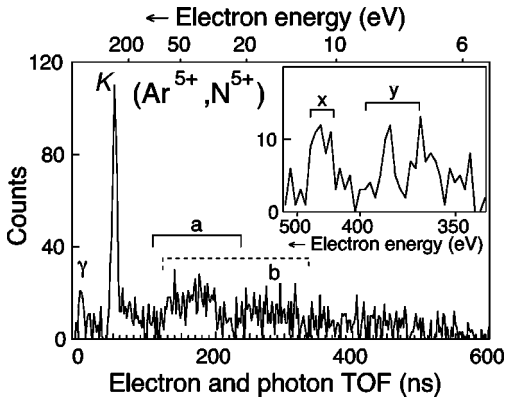

FIG. 9. A partial Auger-electron/photon spectrum in coincidence with the (Ar^{5+}, N^{5+}) ion pair. Inset: A moderate resolution *K*-Auger-electron spectrum in coincidence with the same ion pair. The labels correspond to the following Auger transitions: *a*: $(3,3,3,3,3)\rightarrow(2,3,3,3)$; *b*: $(2,3,3,3)\rightarrow(2,2,3)$; *x*: $(2,2,3)\rightarrow(1,2)$; *y*: $(2,2,3)\rightarrow(1,3)$. The electron TOF ranges, in the main spectrum, are shown in solid lines for the first autoionization steps and in dashed lines for the second autoionization steps.

IV. SUMMARY

A. Double-electron capture

Double-electron capture mainly populates the $(3,n=3-5)$ and $(4,n=4,5)$ configurations. The ECB model [62] accounts for all the observed configurations provided four-electron strings are used, and the relative intensities of the different configurations are reasonably accounted for. The population of the $(3,n=3-5)$ configurations is accompanied by significant target excitation in support of the predictions of the ECB model. No *K*-Auger electrons have been observed following double-electron capture. There is a strong reason to believe that P_{rad} for the $(3,n>9)$ Rydberg series at a given collision energy, following population transfer from the (4,4) configuration via the ATR mechanism, is larger than reported in the literature at that energy (see, e.g., [76,77]). This is in favor of the ATR model that takes into account the increase of the angular momentum of the Rydberg electron [79].

B. Triple-electron capture

Triple-electron capture is found to mainly populate the $(3,3,n=3-5)$ and $(3,4,n=4,5)$ configurations. The former are believed to be accompanied by target excitation. These configurations can be accounted for by the ECB model, but the relative intensities are not well accounted for. No *K*-Auger electrons are found in coincidence with the (Ar^{3+}, N^{5+}) ion pair, indicating that they are not emitted in the first autoionization step. It is found that retention of one or two electrons by the projectile is mainly determined by the competition between the radiative and autoionization decay modes of doubly excited daughter configurations of the form $(2,n=3-5)$. These configurations are found to have large

average fluorescence yields. The role played by the ATR mechanism in retaining two electrons is not found to be as important as reported by Roncin *el al.* [39]. Clear deviations from the criterion of autoionization to the nearest continuum limits have been observed for the $(3,3,n=4,5)$ configurations. Their combined autoionization branching ratio to the $(2,n=4,5)$ continuum limits is about 0.72 while that to the (2,3) limits is about 0.28.

C. Quadruple-electron capture

Quadruple-electron capture mainly populates the $(3,3,3,n=3,4)$ and (3,3,4,4) configurations, in agreement with the predictions of the ECB model. *K*-Auger electrons are found in coincidence with both the (Ar^{4+}, N^{6+}) and the (Ar^{4+}, N^{5+}) ion pairs. Retention of two electrons by the projectile is realized following two main pathways; by the radiative stabilization of ''third generation'' doubly excited configurations of the form $(2,n=2-4)$, and by the filling of a *K*-shell vacancy in the autoionization process of triply excited daughter configurations of the form $(2,3,n=3,4)$. The latter pathway represents significant deviations from the criterion of autoionization to the nearest continuum limits, and calls for theoretical investigations of the radiative and nonradiative properties of the $(2,3,n=3,4)$ configurations.

D. Quintuple-electron capture

Quintuple-electron capture dominantly populates the (3,3,3,3,3) configuration, in agreement with the prediction of the ECB model. It results in the retention of only two electrons by the projectile. The majority of the low-energy and *K*-Auger electrons can indeed be traced to this initial configuration.

V. CONCLUSIONS

We have presented triple-coincidence measurements of Auger electrons, scattered projectile, and target recoil ions in the 70-keV $^{15}N^{7+}$ + Ar collision system. The measurements provided subpartial Auger-electron spectra corresponding to specific pairs of final projectile and recoil-ion charge states. The spectra were discussed within the framework of the extended classical overbarrier model by Niehaus [62]. The model accounted reasonably well for the initial populations for double- through quintuple-electron capture, assuming simultaneous target excitation in many cases. Relaxation pathways for the multiply excited configurations have been suggested with the aid of the experimental data and simple arguments. For this collision system, *K*-Auger electrons are generally emitted in the second or third step of an autoionizing cascade and not in the first step. Deviations from the widely adopted criterion of autoionization to the nearest continuum limits have been observed. In some cases, it was possible to estimate Auger yields and branching ratios for autoionization to different continuum limits. The ATR mechanism plays an important role in the stabilization of both electrons following double-electron capture into the (4,4) configuration. It does not seem, however, to be as important in triple- through quintuple-electron capture processes. Further theoretical investigations of the radiative and nonradiative properties of multiply excited states are clearly needed if some of the experimental observations are to be better understood.

Note added in proof. Since the submission of this article, another coincident Auger-electron spectroscopy study of the same collision system studied in this work, using a technique similar to that used in [53–57], has been reported by Moretto-Capelle *et al.* [83].

ACKNOWLEDGMENTS

E.D.E. acknowledges the support of the U.S. DOE. This work was supported by the NSF under Grant No. PHY-9732614.

[1] E.K. Janev and H. Winter, Phys. Rep. **117**, 265 (1985).
[2] M. Barat and P. Roncin, J. Phys. B **25**, 2205 (1992).
[3] C.L. Cocke, in *Review of Fundamental Processes and Applications of Atoms and Ions*, edited by C.D. Lin (World Scientific, Singapore, 1993), p. 111.
[4] V. Mergel *et al.*, Phys. Rev. Lett. **74**, 2200 (1995).
[5] A. Cassimi *et al.*, Phys. Rev. Lett. **76**, 3679 (1996).
[6] X. Flechard *et al.*, J. Phys. B **30**, 3697 (1997).
[7] M.A. Abdallah *et al.*, Phys. Rev. A **57**, 4373 (1998).
[8] M.A. Abdallah *et al.*, Phys. Rev. A **58**, 2911 (1998).
[9] J.W. McGowan and L. Kerwin, Can. J. Phys. **45**, 1451 (1967).
[10] H.J. Zwally and D.W. Koopman, Phys. Rev. A **2**, 1851 (1970).
[11] H. Klinger, A. Müller, and E. Salzborn, J. Phys. B **8**, 230 (1975).
[12] L.D. Gardner *et al.*, Phys. Rev. A **20**, 766 (1979).
[13] J. Aubert *et al.*, Phys. Rev. A **22**, 2403 (1980).
[14] J. Vancura *et al.*, Phys. Rev. A **49**, 2515 (1994).
[15] R. Ali *et al.*, Phys. Rev. A **49**, 3586 (1994).
[16] N. Nakamura *et al.*, J. Phys. B **28**, 2959 (1995).
[17] N. Selberg, C. Biedermann, and H. Cederquist, Phys. Rev. A **56**, 4623 (1997).
[18] K. Suzuki, K. Okuno, and N. Kobayashi, Phys. Scr. **T73**, 172 (1997).
[19] H.A. Sakaue *et al.*, Phys. Scr. **T73**, 182 (1997).
[20] C.L. Cocke *et al.*, Phys. Rev. Lett. **46**, 1671 (1981).
[21] E. Justiniano *et al.* Phys. Rev. A **24**, 2953 (1981).
[22] G. Astner *et al.*, J. Phys. B **17**, L877 (1984).
[23] L. Liljeby *et al.*, Phys. Scr. **33**, 310 (1986).
[24] H. Danared *et al.*, Phys. Scr. **36**, 756 (1987).
[25] H. Cederquist *et al.*, Nucl. Instrum. Methods Phys. Res. B **24/25**, 43 (1987).
[26] A. Delon *et al.*, Radiat. Eff. Defects Solids **126**, 337 (1993).
[27] J. Bernard *et al.*, Phys. Scr. **56**, 26 (1997).
[28] W. Groh *et al.*, J. Phys. B **16**, 1997 (1983).
[29] I. Yamada *et al.*, J. Phys. B **28**, L9 (1995).
[30] S. Duponchel *et al.*, Nucl. Instrum. Methods Phys. Res. B **98**, 288 (1995).
[31] M.L.A. Raphaelian *et al.*, Phys. Rev. A **51**, 1304 (1995).

[32] J. Vancura, V. Marchetti, and V.O. Kostroun, in *Proceedings of the VIth International Conference on the Physics of Highly Charged Ions*, edited by P. Richard, M. Stöckli, C.L. Cocke, and C.D. Lin, AIP Conf. Proc. **274** (AIP, New York, 1993), p. 113.
[33] G. de Nijs *et al.*, J. Phys. B **29**, 85 (1996).
[34] P. Roncin *et al.*, Europhys. Lett. **3**, 53 (1987).
[35] P. Hvelplund *et al.*, J. Phys. B **20**, 2515 (1987).
[36] H. Anderson *et al.*, Phys. Scr. **42**, 150 (1990).
[37] R. Ali *et al.*, Phys. Rev. Lett. **69**, 2491 (1992).
[38] M. Sakurai *et al.*, in *Proceedings of the VIth International Conference on the Physics of Highly Charged Ions* (Ref. [32]), p. 101.
[39] P. Roncin *et al.*, Nucl. Instrum. Methods Phys. Res. B **98**, 275 (1995).
[40] J. Bernard *et al.*, Phys. Scr. **T73**, 190 (1997).
[41] H. Danared *et al.*, J. Phys. B **20**, L165 (1987).
[42] H. Schmidt-Böcking *et al.*, Phys. Rev. A **37**, 4640 (1988).
[43] L. Guillemot *et al.*, J. Phys. B **23**, 4293 (1990).
[44] R. Herrmann *et al.*, Phys. Rev. A **46**, 5631 (1992).
[45] R. Ali *et al.*, J. Phys. B **26**, L685 (1993).
[46] S. Martin *et al.*, Phys. Rev. Lett. **64**, 2633 (1990).
[47] S. Martin *et al.*, Phys. Rev. A **42**, 6564 (1990).
[48] S. Martin *et al.*, Phys. Lett. A **165**, 441 (1992).
[49] S. Martin *et al.*, Phys. Rev. Lett. **77**, 4306 (1996).
[50] A. Bordenave-Montesquieu *et al.*, Nucl. Instrum. Methods Phys. Res. B **23**, 94 (1987).
[51] P. Benoit-Cattin *et al.*, J. Phys. B **21**, 3387 (1988).
[52] J. Vancura, P.J. Mucha, and V.O. Kostroun, Phys. Rev. A **53**, 2379 (1996).
[53] J.H. Posthumus and R. Morgenstern, Phys. Rev. Lett. **68**, 1315 (1992).
[54] J.H. Posthumus and R. Morgenstern, J. Phys. B **25**, 4533 (1992).
[55] G. de Nijs, R. Hoekstra, and R. Morgenstern, J. Phys. B **27**, 2557 (1994).
[56] G. de Nijs, R. Hoekstra, and R. Morgenstern, Nucl. Instrum. Methods Phys. Res. B **98**, 307 (1995).
[57] G. de Nijs, R. Hoekstra, and R. Morgenstern, J. Phys. B **29**, 6143 (1996).
[58] H. Merabet *et al.*, Phys. Rev. A **59**, R3158 (1999).
[59] H. Merabet *et al.*, in *Proceedings of the Fifteenth International Conference on the Application of Accelerators in Research and Industry*, edited by J.L. Duggan and I.L. Morgan, AIP Conf. Proc. No. 475 (AIP, New York, 1999), p. 99.
[60] H. Ryufuku, K. Sasaki, and T. Watanabe, Phys. Rev. A **21**, 745 (1980).
[61] A. Bárány *et al.*, Nucl. Instrum. Methods Phys. Res. B **9**, 397 (1985).
[62] A. Niehaus, J. Phys. B **19**, 2925 (1986).
[63] N. Vaeck and J.E. Hansen, J. Phys. B **25**, 3267 (1992).
[64] N. Vaeck and J.E. Hansen, J. Phys. B **28**, 3523 (1995).
[65] H. Bachau, J. Phys. B **29**, 4365 (1996).
[66] H. Bachau, in *Proceedings of the Fourteenth International Conference on the Application of Accelerators in Research and Industry*, edited by J.L. Duggan and I.L. Morgan, AIP Conf. Proc. 392 (AIP, New York, 1997), p. 273.
[67] B.C. Gou and K.T. Chung, J. Phys. B **29**, 6103 (1996).
[68] Y. Zhang and K.T. Chung, Phys. Rev. A **58**, 1098 (1998).
[69] Y. Azuma *et al.*, Phys. Rev. Lett. **74**, 3768 (1995).
[70] L. Journel *et al.*, Phys. Rev. Lett. **76**, 30 (1996).
[71] S. Diehl *et al.*, Phys. Rev. Lett. **79**, 1241 (1997).
[72] J.-Y. Chesnel *et al.*, Phys. Rev. A **57**, 3546 (1998).
[73] B. Jacquot and M. Pontonnier, Nucl. Instrum. Methods Phys. Res. A **287**, 341 (1990).
[74] R.D. Cowan, *The Theory of Atomic Structure and Spectra* (University of California Press, Berkeley, CA, 1981).
[75] A.A. Hasan *et al.*, Phys. Rev. Lett. (to be published).
[76] P. Roncin, M.N. Gaboriaud, and M. Barat, Europhys. Lett. **16**, 551 (1991).
[77] P. Roncin *et al.*, J. Phys. B **26**, 4181 (1993).
[78] H. Bachau, P. Roncin, and C. Harel, J. Phys. B **25**, L109 (1992).
[79] A.K. Kazansky and P. Roncin, J. Phys. B **27**, 5537 (1994).
[80] H. Merabet *et al.*, Phys. Rev. A **54**, 372 (1996).
[81] N. Stolterfoht *et al.*, Phys. Rev. A **42**, 5396 (1990).
[82] Y. Hahn , in *Proceedings of the Thirteenth International Conference on the Physics of Electronic and Atomic Collisions*, edited by J. Eichler, I.V. Hertel, and N. Stolterfoht (North-Holland, Amsterdam, 1983), p. 801.
[83] P. Moretto-Capelle, D. Bordenave-Montesquieu, and A. Bordenave-Montesquieu, Phys. Scr. **T80**, 118 (1999).